Springer

KSME

Journal of Mechanical Science and Technology 25 (6) (2011) 1603~1611
www.springerlink.com/content/1738-494x
DOI 10.1007/s12206-011-0334-y

Accurate calibration of kinematic parameters for two wheel differential mobile robots †

Kooktae Lee, Changbae Jung and Woojin Chung*

School of Mechanical Engineering, Korea University, Seoul, 136-701, Korea

(Manuscript Received October 19, 2010; Revised March 23, 2011; Accepted March 29, 2011)

Abstract

Odometry using wheel encoders provides fundamental pose estimates for wheeled mobile robots. Systematic errors of odometry can be reduced by the calibration of kinematic parameters. The UMBmark method is one of the widely used calibration schemes for two wheel differential mobile robot. In this paper, an accurate calibration scheme of kinematic parameters is proposed by extending the conventional UMBmark. The contributions of this paper can be summarized as two issues. The first contribution is to present new calibration equations that remarkably reduce the systematic error of odometry. The new equations were derived to overcome the limitation of the conventional schemes. The second contribution is to propose the design guideline of the test track for calibration experiments. The calibration performance can be significantly improved by appropriate design of the test track. The numerical simulations and experimental results show that the odometry accuracy can be improved by the proposed calibration schemes.

Keywords: Calibration; Localization; Mobile robots; Odometry; Systematic errors

1. Introduction

Odometry using wheel encoders provides fundamental pose estimates for wheeled vehicles. The major drawback of odometry is the accumulation of errors. Odometry error sources can be divided into two different groups as illustrated in [1-3]. The first source is systematic error, which is deterministic. Systematic error sources include unequal wheel diameters, misalignment of wheels, or kinematic modeling errors. Therefore, it is desirable to reduce the systematic error through appropriate calibration of kinematic parameters.

The second source is nonsystematic error, which is stochastic. Nonsystematic errors mainly result from environmental conditions such as an uneven ground or wheel slippage. Therefore, nonsystematic errors are described in terms of probability, for example, as in Ref. [4]. Since uncertainty of pose estimation grows according to the increase of the travel distance, external sensors are used for correcting the robot pose. Bento [5] and Surrecio [6] proposed nonsystematic error reduction methods by combining odometry and external magnetic sensor data.

There have been some calibration schemes to compensate for systematic errors. Tonouchi [7] suggested a pose estimation algorithm by means of Bayesian inference where the dead-reckoning position and the exact workspace model are fused. Komoriya [8] introduced a calibration method using the optical fiber gyroscope sensor. Doh [9] proposed a PC-method using path odometry information. The robot follows a GVG path for calibration. The scheme in Ref. [9] is applicable for all wheel structures. Ivanjko introduced a simple off-line calibration method in Ref. [10]. The final robot poses were measured with respect to artificial landmarks and on-line adaptation was possible. Abbas proposed the bi-directional circular path test (BCPT) in Ref. [11]. Bostani [12] introduced a simple method for measurement and calibration of odometry errors. The calibration scheme was built on the basis of the scaling error E_s that is the difference between the average and the nominal wheel diameter.

There have been many useful calibration schemes for various wheel mechanisms including two wheel differential wheels, synchronous wheels and car-like mobile robots as in Refs. [1, 3-14]. This paper deals with two wheel differential mobile robots. Two wheel robots are advantageous because of simple mechanical structures and controllers. The typical approaches for calibration of two wheel robots can be found in Ref. [1].

The UMBmark [1] is a widely used scheme. Since the calibration is completed just by measuring the final position after a sequence of open loop motions, practical implementation is easy. This paper proposes a new calibration strategy by ex-

† This paper was recommended for publication in revised form by Associate Editor Won-Gu Lee

* Corresponding author. Tel.: +82 2 3290 3375, Fax.: +82 2 3290 3375
E-mail address: smartrobot@korea.ac.kr

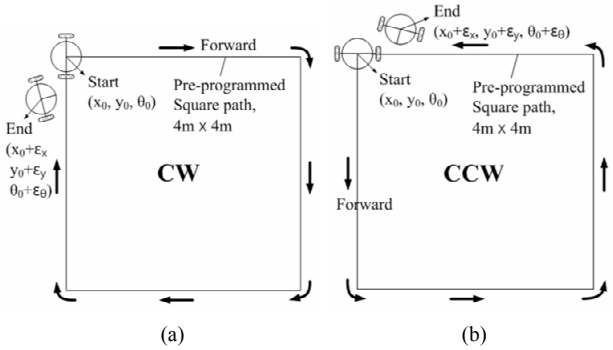

Fig. 1. The calibration experiments by the open loop motion control along the square path to CW and CCW directions in UMBmark [1].

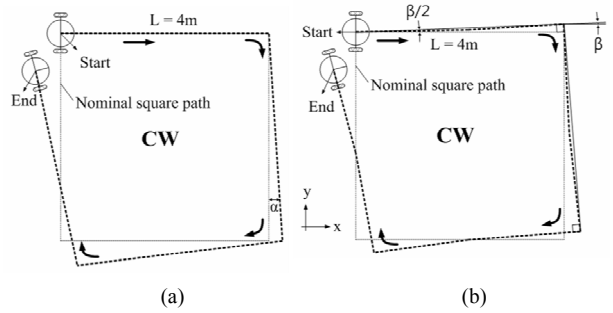

Fig. 2. Illustration of end position errors by type A and type B errors.

tending the conventional UMBmark.

Our first objective is to derive a new accurate calibration scheme after investigating the limitation of the conventional UMBmark. The calibration strategy in Ref. [1] was derived under the assumption that the wheel radius error and the wheelbase error are completely independent. The new calibration equations in this paper are derived under the investigation of coupled effect between the wheel radius error and the wheelbase error.

The second objective is to present the design guideline of the test track for calibration experiments. From experience, the authors recognized that the calibration performance can be significantly improved by appropriate design of the test track. The presented numerical simulations show that the appropriate selection of the track size is essential to improve the calibration accuracy.

This paper is organized as follows. Section 2 revisits the UMBmark in Ref. [1] and proposes new calibration equations. The requirements of the track design are explained. In section 3, we investigate the advantage of the proposed calibration scheme and the importance of the track design through numerical simulations. Experimental verifications are shown in section 4.

2. Accurate calibration of kinematic parameters

2.1 Illustration of the UMBmark in Ref. [1]

Fig. 1 shows the experimental motion that was proposed in

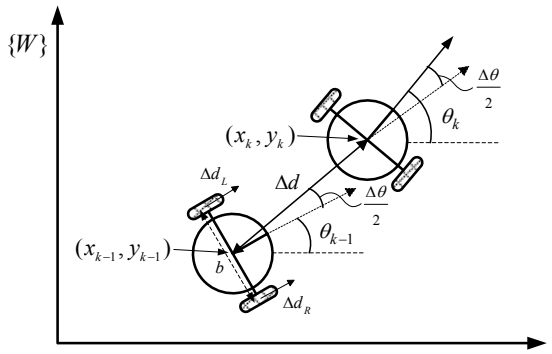

Fig. 3. The kinematic model of a two wheel differential mobile robot.

UMBmark [1]. Two sources of systematic errors were assumed: wheel radius error and wheelbase error. In Ref. [1], it was assumed that two error sources independently affect the final positional errors of a robot. Two kinematic parameters are calibrated from positional errors.

Fig. 2 illustrates the effect of kinematic parameter errors. Type A errors affect the orientation error during the rotating motion at corners as shown in Fig. 2(a). Type A errors are caused by the wheelbase modeling error. Fig. 2(b) shows curved paths because of the wheel radius modeling error. The curved motion causes type B error that result from the wheel radius modeling error.

The final position of the robot is determined through highly nonlinear equations. Furthermore, there is a coupled effect between the radius error and the wheelbase error. In a strict sense, the principle of superposition in Ref. [1] is invalid. We propose a new calibration equation under the consideration of the simultaneous occurrence of type A and B errors.

2.2 New calibration equations by considering the coupled effect of wheelbase errors and unequal wheel diameters

The kinematic model of a mobile robot is shown in Fig. 3. The odometry pose of a differential drive robot can be computed by following equations as in Ref. [13]:

$$\begin{aligned} x_k &= x_{k-1} + \Delta d \cdot \cos(\theta_{k-1} + \Delta\theta/2) \\ y_k &= y_{k-1} + \Delta d \cdot \sin(\theta_{k-1} + \Delta\theta/2) \\ \theta_k &= \theta_{k-1} + \Delta\theta \end{aligned} \tag{1}$$

$$\Delta d = \frac{\Delta d_R + \Delta d_L}{2} \tag{2}$$

$$\Delta\theta = \frac{\Delta d_R - \Delta d_L}{b} \tag{3}$$

$$\Delta d_{R(L)} = \pi D_{R(L)} \frac{N_{R(L)}}{\mathrm{Re}_{R(L)}} \tag{4}$$

x_k : Position of the robot in the x-direction at time k,
y_k : Position of the robot in the y-direction at time k,
θ_k : Heading direction of the robot at time k,
$\Delta d_{r(l)}$: Incremental displacement of the right and left wheels,

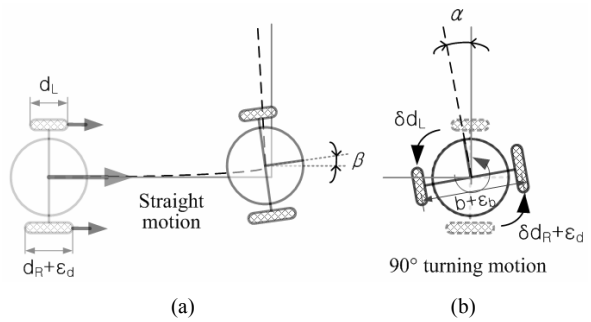

Fig. 4. The occurrence of pose errors because of wheel radius errors and wheelbase errors (a) Heading error β after translation; (b) Heading error α after rotation.

$\Delta\theta$: Incremental heading angle for the robot,
$D_{r(l)}$: Nominal diameter of the right (left) wheel,
$N_{r(l)}$: The number of encoder pulses of the right (left) wheel,
$Re_{r(l)}$: Encoder resolution of the right(left) wheel.

To investigate the coupled effect between the wheel radius and wheelbase errors, we assume that two errors occur simultaneously. Fig. 4 shows that the orientation errors after a straight motion and a 90° turning motion in CCW direction. The initial robot heading is 0°. The resultant robot orientation may contain some errors because of wheel radius error as well as wheelbase error. The simultaneous occurrence of two errors was not considered in Ref. [1].

When the right wheel radius is larger than the radius of a left wheel as ε_d, orientation error β takes place after a translational motion by 4m as shown in Fig. 4(a). The heading error β for *m* encoder pulses can be computed as the following equation:

$$\beta = \sum_{i=1}^{m} \frac{((\Delta d_R + \varepsilon_d) - \Delta d_L)}{b} = \sum_{i=1}^{m} \frac{\varepsilon_d}{b} = \frac{\varepsilon_d \cdot m}{b}. \tag{5}$$

Incremental displacements Δd_R and Δd_L can be obtained from Eq. (4). Fig. 4(b) shows the robot pose before the turn (gray) and the robot pose after the turn (black). The resultant heading after 90° rotational motion for *n* encoder pulses can be computed as a following equation:

$$\theta_{actual} = \sum_{i=1}^{n} \frac{((\Delta d_R + \varepsilon_d) - (-\Delta d_L))}{b + \varepsilon_b}. \tag{6}$$

From Eq. (6), it can be seen that the orientation error after a 90° turn is caused by the coupled effect of the wheelbase error ε_b and wheel radius error ε_d. From Eq. (6), the following equation is derived:

$$\theta_{actual} = \sum_{i=1}^{n} \frac{(\Delta d_R - (-\Delta d_L))}{b + \varepsilon_b} + \sum_{i=1}^{n} \frac{\varepsilon_d}{b} = 90^\circ + \alpha. \tag{7}$$

Therefore, the orientation error α for 90° rotational motion is newly defined as follows:

$$\alpha = \alpha_{\varepsilon_b} + \alpha_{\varepsilon_d}. \tag{8}$$

α_{ε_b} is caused by the wheelbase error. To compute α_{ε_d} in Eq. (8), translational displacement L and angular displacement $\theta_{nominal}$ can be derived as follows:

$$L = \sum_{i=1}^{m} \frac{((\Delta d_R + \varepsilon_d) + \Delta d_L)}{2} = (\Delta d + \frac{\varepsilon_d}{2}) \cdot m$$
$$\theta_{nominal} = \sum_{i=1}^{n} \frac{(\Delta d_R + \Delta d_L)}{b} = -\frac{2\Delta d \cdot n}{b}. \tag{9}$$

Finally, α_{ε_d} can be computed as follows:

$$\alpha_{\varepsilon_d} = -\frac{\pi}{4} \cdot \frac{b\beta}{(L - \frac{b\beta}{2})}. \tag{10}$$

According to the result in Eq. (10), the calibration equations can be rewritten as follows:

$$\alpha = \frac{x_{cw} + x_{ccw}}{-4L} + \frac{\pi b}{4\left(\frac{-4L^2}{x_{cw} - x_{ccw}} - \frac{b}{2}\right)} \tag{11}$$

or

$$\alpha = \frac{y_{cw} - y_{ccw}}{-4L} + \frac{\pi b}{4\left(\frac{-4L^2}{y_{cw} + y_{ccw}} - \frac{b}{2}\right)}. \tag{12}$$

The first terms in Eqs. (11), (12) are identical to the equations in Ref. [1]. The second terms are newly added in this paper.

2.3 Design of the test track

One of the significant factors of odometry calibration is the design of the test track. The shape of the test track is identical to the square path in Ref. [1]. However, there are no considerations on the size of the track in Ref. [1]. The size of the test track was 4mx4m without detailed explanation. The authors recognized that the size of the track plays a significant role in experiments. The size of the test track should be carefully determined under the consideration of the wheel radius, the kinematic modeling error and the calibration equations.

When the track is too large, huge experimental space is required. In addition, pose error α in Eqs. (11), (12) becomes too large. This fact implies that the approximations $\sin\alpha = \alpha$, $\cos\alpha = 1$ become invalid.

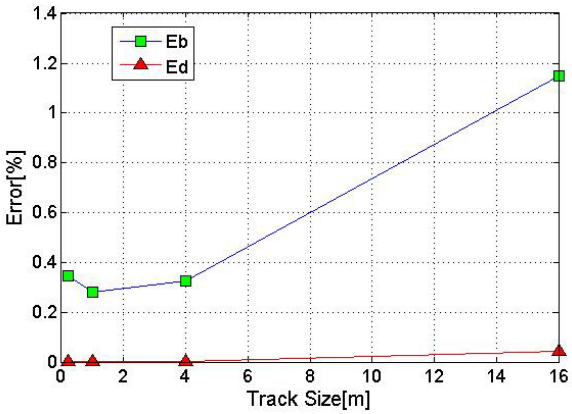

(a) E_b and E_d (Conventional UMBmark)

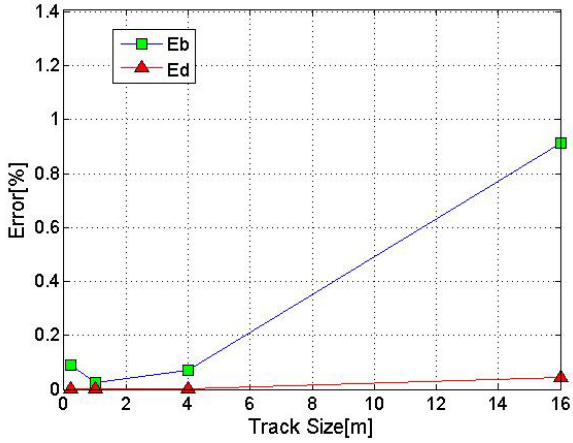

(b) E_b and E_d (Proposed calibration scheme)

Fig. 5. Kinematic parameter errors after calibration along four different tracks L = 0.2, 1, 4, 16m.

On the other hand, too small tracks may result in too small final pose errors, which implies that the calibration results become too sensitive with respect to the measurement accuracy of robot positions. Therefore, the size of the test track is a significant experimental issue. For the calibration problem of a car-like mobile robot, the design guidelines and considerations are presented in Refs. [14-16].

3. Simulations

The aim of the numerical simulation is to clarify two contributions of the proposed calibration strategy. The first objective is to show the advantage of the presented calibration scheme in Eqs. (11), (12). The second objective is to establish the design guideline of a test track. Nonsystematic errors were excluded from the numerical simulations because the major scope is to investigate the effect of systematic errors.

In simulations, the robot pose is numerically computed from the robot kinematics under kinematic modeling errors. The calibration performance is evaluated by the difference between the real and the estimated E_b and E_d. Fig. 5 shows the resultant error of E_b and E_d under four different track sizes.

Fig. 6. The robot used in experiments.

The track size is denoted by the length of a side of a square L. Four selected tracks were L = 0.2, 1, 4, 16m. Since y represents the kinematic modeling error after calibration, smaller y is preferable.

The initial condition was E_b = 1.010, E_d = 0.995. Fig. 5(a) shows the calibration result by the use of the conventional UMBmark. It can be seen that the parametric errors increase when the track size is too large. This result coincides with the comments in section 2.3. The large parametric errors resulted from the invalid approximation $\sin\alpha = \alpha$, $\cos\alpha = 1$ because α is too large. From Fig. 5(a), it is recommended to choose $L \leq 4$m.

From Fig. 5(a), it is clear that E_b still contains parametric error after calibration, while E_d can be accurately calibrated. The error source of E_b is the coupled effect of two error sources as explained in section 2.2.

Fig. 5(b) shows the calibration result on the basis of the proposed calibration scheme in Eqs. (11), (12). It is clear that parametric errors of E_b become remarkably smaller than in Fig. 5(a), which implies that the simultaneous occurrence of two errors should be modeled in the calibration equation. The resultant E_b was 1.0128 under the conventional UMBmark in Fig. 5(a). The resultant E_b was 1.0103 by the proposed scheme in Fig. 5(b). The parametric error after calibration decreased from 0.28% (conventional) to 0.03% (proposed). This result shows that the calibration accuracy was improved by 10 times when the proposed scheme was applied.

4. Experimental results

4.1 Experimental setup

Fig. 6 shows the commercially available mobile robot from Ref. [17] for experiments. The robot is driven by two independent wheel actuators. The nominal dimensions are given as D = 150mm, b = 385mm and the width of a tire is 30mm. Each wheel is equipped with optical encoders and the resolution is 200,000 pulses/rev. The experimental robot poses were

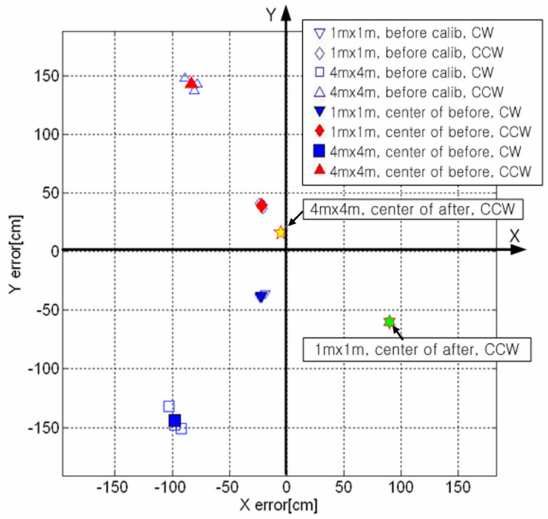

Fig. 7. Calibration results by the proposed scheme. The final pose errors decreased after calibration.

monitored by the use of a commercially available STARGAZER system in Ref. [18].

4.2 Calibration experiments and performance comparison

The robot is driven by open loop control along the square path. The moving directions of a robot should include both CW and CCW. Two track sizes were tested for L = 1m and L = 4m. To investigate the effect of both systematic and nonsystematic errors, the robot should be driven multiple times under the same condition. The geometric center of final poses under the same condition represents the final pose under the systematic errors. If the calibration is successful, the final pose after calibration converges to the origin. The pose distribution around the center represents the stochastic nonsystematic error. The final poses during the calibration experiments are plotted in Fig. 7.

From Fig. 7, it can be seen that the final pose error along the 4mx4m path is greater than the pose error along the 1mx1m path. This is natural because the final pose error is accumulated when the traveling distance increases under the same systematic errors. The first experiment was carried out for the 4mx4m path. From the final pose errors before calibration, E_b and E_d are computed. Then, the robot is driven again. It is evident that the final odometry pose after calibration is (x, y) = (-5cm, 16cm), which is close to the origin in Fig. 7. This result clearly shows that the proposed calibration scheme is useful in practical applications.

To investigate the effect of the track size, a robot is driven along the 1mx1m path. Although the final pose before calibration was small, the final pose after calibration was (x, y) = (90cm, -60cm), which shows large pose error in Fig. 7. For comparison, the final pose after calibration was commonly tested for the 4mx4m path. This fact implies that the calibration process for the 1mx1m path was not successful because the track size was too small, as mentioned in section 2.3. On the other hand, the test track should not be too large, as explained in section 3.

Table 1. Parameters of simulations and experiments.

	Track length	Before Calibration	After Calibration
UMBmark Method	2mx2m		10.99 cm
	4mx4m	146.14 cm	34.97 cm
Proposed Method	2mx2m		6.79 cm

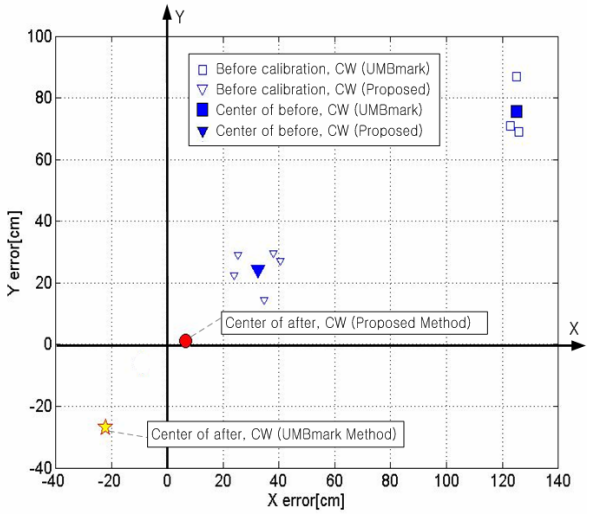

Fig. 8. Comparison between the proposed and the conventional calibration schemes. The final pose error of the proposed scheme is smaller.

From experience, we found that the appropriate size of the test track is 2mx2m path under the present experimental conditions. Therefore, our proposal can be summarized as the new calibration equations in Eqs. (11), (12) together with the 2mx2m path. The second calibration experiments were performed for comparison between the proposed and the conventional calibration schemes.

The experimental results are presented in Fig. 8 and Table 1. The final positional error before calibration was 146.14 cm. After application of the conventional UMBmark in Ref. [1], the error was reduced to 34.97cm. Therefore, the odometry accuracy was increased by four times by the UMBmark.

The final pose error after the application of the proposed scheme was 6.79cm. The odometry accuracy of the proposed scheme is five times higher than the conventional UMBmark approach. This result clearly shows the advantage of the proposed calibration scheme over the prior approach.

Fig. 9 visually summarizes the comparison of the odometry errors of presented experimental results. It is clear that the odometry accuracy can be remarkably improved by the proposed scheme.

Since the calibration schemes include approximations, it is interesting to investigate whether the kinematic parameters converge through iterative calibration experiments. In Refs. [14-16], it is shown that kinematic parameters can be itera-

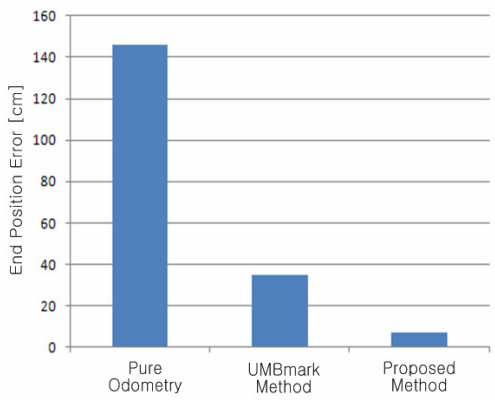

Fig. 9. Comparison of the final pose errors.

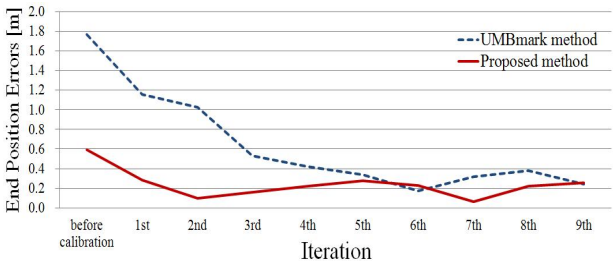

Fig. 10. Convergence of final pose errors by iterative calibration experiments.

tively calibrated for car-like mobile robots.

Iterative calibration experiments were carried out for nine times. The objective was to investigate the convergence of parameters and to compare the proposed scheme with the conventional UMBmark. The initial conditions were set to be identical and the kinematic parameters were updated at the end of each iteration.

Fig. 10 shows the odometry pose errors after each calibration experiment. It is clear that the errors decrease by iteration, implying that the kinematic parameters converge. Since there are various error sources including nonsystematic errors, the errors are hard to vanish completely. We set the threshold error of convergence as 0.3m.

It is clear that the pose error by the proposed scheme converged after the first iteration, while the error by the UMBmark shows slow convergence speed. Therefore, it can be concluded that the proposed scheme is more efficient from the viewpoint of convergence speed.

4.3 Quantitative comparison experiments of odometry accuracy

Calibrated kinematic parameters directly contribute to improvement of odometry accuracy of mobile robots. To clarify the advantage of the proposed calibration scheme, experiments were carried out. The radius of the left wheel is intentionally increased by winding tape around the tire in order to create extreme situations. Approximate difference of radius between the two wheels is 1.5mm. The test track is designed

Table 2. Parameters of simulations and experiments.

Experiment		End Position Errors (m)		
		Raw odometry	UMBmark method	Proposed method
Test Track	1st	5.73	1.47	0.13
	2nd	5.60	1.33	0.05
	3rd	5.60	1.38	0.04
	Average	**5.64**	**1.39**	**0.07**

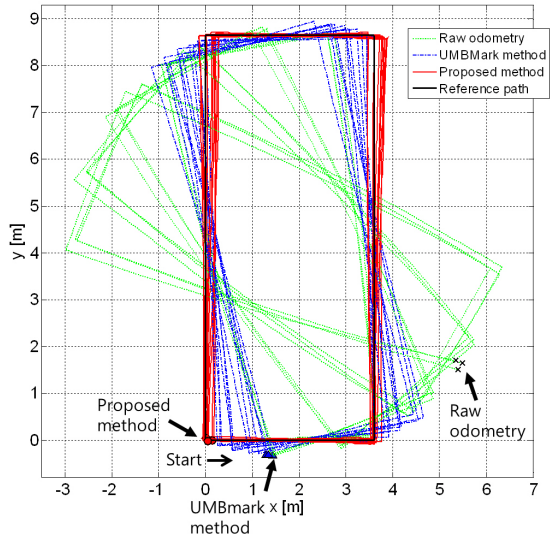

Fig. 11. Comparison of odometry accuracy for three cases (Without calibration / UMBmark / Proposed).

as a 3.6mx8.7m rectangle for simplicity. The translational velocity of the robot is 0.3m/s. The robot makes four CCW round trips from the origin. To monitor nonsystematic errors, three tests were done under the same condition. The resultant parameters by the conventional UMBmark were E_b = 0.9687 and E_d = 0.9927. Calibrated parameters by the proposed scheme were E_b = 0.9762 and E_d = 0.9924.

Fig. 11 shows the experimental results. The robot was manually driven repeatedly along the rectangular reference path. The actual positions of the robot always remain in the rectangular path; however, the odometry path may contain errors due to systematic errors.

From Fig. 11, it can be seen that the final positional errors without calibration are large. The nonsystematic errors are relatively small. Although the final positional error was reduced by the application of the conventional UMBmark, there are still large errors. On the contrary, the final positional errors with the proposed scheme are much smaller than for other results.

Table 2 summarizes the final positional errors. The average positional error was 5.64m before calibration. The error was reduced to 1.39m by the conventional UMBmark. The error was further reduced to 0.07m when the proposed scheme was adopted. The positioning accuracy of the proposed scheme was improved by 20 times better than the UMBmark, and the

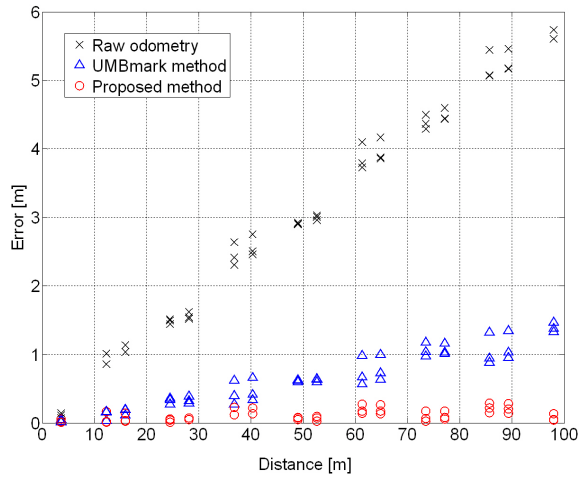

Fig. 12. Increase of odometry errors for three cases (Without calibration / UMBmark / Proposed).

improvement is noteworthy. Fig. 12 shows the odometry errors according to the increase of the traveling distance. It is evident that the increase of odometry error is smallest when the proposed scheme is adopted.

4.4 Experimental comparison of calibration performance

In this section, we compare the calibration performance of the proposed method with previous approaches. Two methods were adopted and tested for comparison: Abbas's BCPT(Bi-directional circular path test) method [11] and Bostani's method [12]. In the BCPT method, the robot is driven along a circular reference path in both *CW* and *CCW* directions, as shown in Fig. 13(a). During the experiment, resultant radii R_{cw} and R_{ccw} of the circular paths are measured. The radii are used for calibration of systematic errors of odometry.

In Bostani's method, the Desired path is a straight line. A robot is driven back and forth, as shown in Fig. 13(b). On-the-spot rotations are required in both CW and CCW directions at the end of the straight line. γ_1 and γ_2 in Fig. 13(b) are experimentally measured. Measured γ_1 and γ_2 are used for calibration of systematic errors. In practice, γ_1 and γ_2 are much smaller than γ_1 and γ_2 in Fig. 13(b).

To reduce the effect of nonsystematic errors, we repeated each experiment for five times. The two wheel differential mobile robot in Ref. [17] and commercially available STARGAZER system [18] were used in experiments.

The resultant error parameters from experiments are listed in Table 3. From Table 3, it is clear that three methods resulted in different parameters. To investigate the accuracy of calibration, the robot was driven along the 4mx4m square path. For each kinematic parameter, a robot was driven five times.

Fig. 14 shows the measured positional errors at the end of experiments. The average positional error was 1.06m before calibration. The final position errors were reduced to 0.44m (BCPT method), 0.42m (Bostani's method) and 0.07m (proposed method), respectively. After calibration, the final posi-

Table 3. The error parameters of the differential mobile robots from BCPT method, Bostani's method and proposed method.

	BCPT method	Bostani's method	Proposed method
E_b	0.9662	0.9683	0.9793
E_d	0.9890	0.9823	0.9876

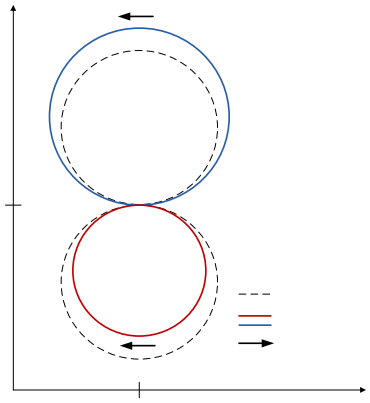

(a) BCPT method

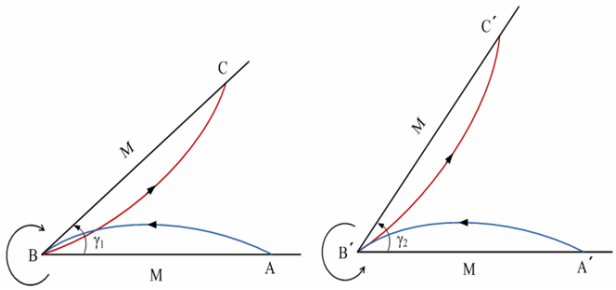

(b) Bostani's method

Fig. 13. The illustration of experimental paths for the BCPT method [11] and the Bostani's method [12].

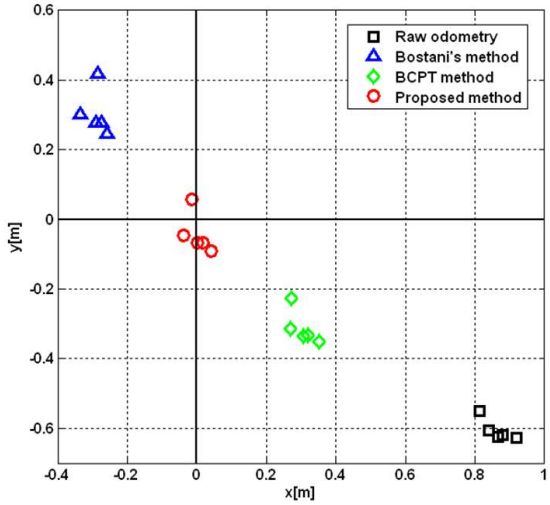

Fig. 14. The final position errors after navigating 4mx4m square path (Without calibration / Bostani's method / BCPT method / Proposed method).

tion errors were reduced by the application of calibration schemes. It is evident that the accuracy of the proposed calibration scheme was highest out of three methods.

5. Conclusion

This paper proposed a new odometry calibration scheme to improve odometry accuracy of two wheel differential mobile robots. The first contribution is to derive new calibration equations by considering the coupled effect of diameter and wheelbase errors. The presented simulations and experiments clearly showed that the proposed scheme provides more accurate calibration results than the conventional scheme. The second contribution was the suggestion of the appropriate size of the test track for calibration. The proposed scheme was experimentally verified and the advantages were clearly shown through quantitative comparison. The proposed calibration scheme is expected to improve the accuracy of mapping and localization, for example, in Refs. [19-22].

Acknowledgment

This work was supported in part by the MKE under the Human Resources Development Program for Convergence Robot Specialists. This work was also supported in part by Basic Science Research Program through the NRF funded by the MEST (2010-0022609).

References

[1] J. Borenstein and L. Feng, Correction of systematic odometry errors in mobile robots, *IEEE International Conference on Intelligent Robots and Systems*, Pittsburgh, PA (1995) 569-574.

[2] Thrun et al., *Probabilistic robotics,* The MIT Press (2005).

[3] Borenstein et al., Where am I? sensors and methods for mobile robot positioning, University of Michigan, Department of Mechanical Engineering and Applied Mechanics, Mobile Robotics Laboratory, 1101 Beal Avenue, Ann Arbor, MI 48109.

[4] Thrun et al., A probabilistic approach to concurrent mapping and localization for mobile robots, *Machine Learning,* 31 (1998) 29-53.

[5] Bento et al., Sensor fusion for precise autonomous vehicle navigation in outdoor semi-structured environments, *IEEE Int. Conf. on Intelligent Transportation Systems (ITSC2005)*, Basel, Switzerland (2005) 245-250.

[6] Surrécio et al., Fusion of odometry with magnetic sensors using kalman filters and augmented system models for mobile robot navigation*, In IEEE Int. Symposium on Industrial Electronics*, Dubrovnik, Croatia (2005) 1551-1556.

[7] Tonouchi et al., Fusion of dead-reckoning positions with a workspace model for a mobile robot by bayesian inference, *International Conference on Intelligent Robots and Systems,* Munich, Germany (1994) 1347-1354.

[8] K. Komoriya and E. Oyama, Position estimation of a mobile robot using optical fiber gyroscope (OFG), *International Conference on Intelligent Robots and Systems,* Munich, Germany (1994) 143-149.

[9] Doh et al., Accurate relative localization using Odometry, *IEEE International Conference on Robotics and Automation*, Taipei, Taiwan (2003) 1606-1612.

[10] Ivanjko et al., Simple off-line odometry calibration of differential drive mobile robots, *Proceedings of 16th Int. Workshop on Robotics in Alpe-Adria-Danube Region–RAAD*, Ljubljana (2007).

[11] Abbas et al., Measurement and correction of systematic odometry errors caused by kinematics imperfections in mobile robots, *SCIE-ICASE International Joint Conference*, Busan, Korea (2006).

[12] Bostani et al., A novel method to measure and correct the odometry errors in mobile robots, *IEEE Canadian Con ference on Electrical and Computer Engineering*, Niagara Falls, Canada (2008).

[13] R. Siegwart and I. R. Nourbakhsh, *Introduction to autonomous mobile robots,* The MIT Press (2004).

[14] Lee et al., Kinematic parameter calibration of a car-like mobile robot to improve odometry accuracy, *Mechatronics,* 20 (5) (2010) 582-595.

[15] K. Lee and W. Chung, Calibration of kinematic parameters of a car-like mobile robot to improve odometry accuracy, *IEEE International Conference on Robotics and Automation*, Pasadena, CA (2008) 2546-2551.

[16] K. Yoo and W. Chung, Convergence analysis of kinematic parameter calibration for a car-like mobile robot, *IEEE/ASME International Conference on Advanced Intelligent Mechatronics*, Singapore (2009) 740-745.

[17] Mobile robot platform : TETRA_DS(II), http://www.dasarobot.com/, DASAROBOT Co.

[18] Indoor localization system : StarGazer^{TM} HSG-A-02, http://www.hagisonic.com/, HAGISONIC Co.

[19] K.-W. Lee, J.-B. Park and B.-H. Lee, Dynamic localization with hybrid trilateration for mobile robots in intelligent space, *Journal of Intelligent Service Robotics*, 1 (3) (2008) 221-235.

[20] J. Laaksonen and V. Kyrki, Localization in ambiguous environments using multiple weak cues, *Journal of Intelligent Service Robotics*, 1 (4) (2008) 281-288.

[21] H. Je, G. S. Sukhatme and D. Kim, Partially observed distance mapping for cooperative multi-robot localization, *Journal of Intelligent Service Robotics*, 2 (1) (2009) 1-8.

[22] A. Gasparri, S. Panzieri and F. Pascucci, A spatially structured genetic algorithm for multi-robot localization, *Journal of Intelligent Service Robotics*, 2 (1) (2009) 31-40.

Kooktae Lee received his BS and his MS in Mechanical Engineering from Korea University, Korea, in 2006 and 2008, respectively. He is now a Ph.D. student at Texas A&M University, USA. From 2008 to 2009, he was a research engineer at Samsung Electronics. His research interests include field robotics, motion planning and control of unmanned vehicle.

Changbae Jung received his BS in Mechanical Engineering from Korea Military Academy, Seoul, Korea, in 1999 and the MS in Mechanical Engineering from the University of Science & Technology Beijing, Beijing, China, in 2005. He is now a Ph.D. student at Korea University, Seoul, Korea. His primary research interest is wheeled mobile robots.

Woojin Chung received the B.S in Mechanical Design and Production Engineering, Seoul National University, Seoul, Korea, in 1993 and the M.S. and Ph.D. degrees from the Department of Mechano-Informatics, University of Tokyo; in 1995 and 1998, respectively. From 1998 to 2005, he was a Senior Research Scientist with the Korea Institute of Science and Technology, Seoul. Since 2005, he has been with the Department of Mechanical Engineering, Korea University, Seoul. His research interests include the design and control of nonholonomic underactuated mechanical systems, trailer-system design and control, and mobile-robot navigation.